

Maximal violation of Kirchhoff's law in planar heterostructures

Lu Wang (汪璐) ¹, F. Javier García de Abajo,^{1,2} and Georgia T. Papadakis ^{1,*}¹ICFO-Institut de Ciències Fòniques, The Barcelona Institute of Science and Technology, 08860 Castelldefels (Barcelona), Spain²ICREA-Institució Catalana de Recerca i Estudis Avançats, Passeig Lluís Companys 23, 08010 Barcelona, Spain

(Received 18 February 2023; accepted 18 May 2023; published 7 June 2023)

Violating Kirchhoff's law is generally achieved using patterned nonreciprocal materials, where a guided or polaritonic mode that lies outside the light cone, often via gratings, is excited. Here, we describe how nonreciprocity manifests itself in *pattern-free* heterostructures. We demonstrate that a resonant mode in a dielectric spacer separating a nonreciprocal film from a back reflector suffices to maximally violate Kirchhoff's law, and identify the minimal dielectric requirements for such functionality, which are satisfied by currently available materials.

DOI: [10.1103/PhysRevResearch.5.L022051](https://doi.org/10.1103/PhysRevResearch.5.L022051)

Global energy demands call for renewable energy production at the terawatt scale and beyond [1]. Light-harvesting renewable energy approaches, such as solar photovoltaic cells, can reach a performance near thermodynamic limits if the fundamental constraint of Kirchhoff's law of thermal radiation is broken [2,3]. Kirchhoff's law states that a material's absorptivity α ought to equal its thermal emissivity e for every frequency and direction. By violating Kirchhoff's law, one can efficiently redirect emitted photons from one energy converter to another in a concatenated energy-conversion scheme, leading to an ultimate energy conversion efficiency of 93% (Landsberg's limit) [4]. So far, several photovoltaic configurations have been proposed, operating both in reflection [2] and transmission geometries [5,6].

Fundamentally, breaking Kirchhoff's law of thermal radiation requires materials that break reciprocity. This is often realized by applying an external magnetic field to magneto-optical materials, such as InAs [7–9]. Nevertheless, high (tesla-scale) external magnetic field strengths are typically required [9–12], thus resulting in structures that are bulky, expensive, and unsuited to large-scale manufacturing [13]. Hence, the first experimental realization of nonreciprocal emission at mid-infrared (mid-IR) frequencies was reported just last year [10]. In that paper, a guided resonant mode was excited in the Voigt configuration via a grating. This result followed several similar theoretical proposals [12] that considered the excitation of a guided-mode resonance in order to amplify the intrinsic nonreciprocal material response.

To alleviate the requirement of high-magnetic fields, magnet-free nonreciprocal materials, namely Weyl semimetals (WSMs), have been recently explored [14–16]. This

emerging class of quantum materials possesses unique topological properties, leading to magnetic-like effects even in the absence of an external magnetic field [17,18]. Several Weyl semimetals have been already experimentally identified, such as WP_2 , $\text{Y}_2\text{Ir}_2\text{O}_7$, HgCr_2Se_4 , TaAs, and $\text{Co}_3\text{Sn}_2\text{S}_2$ [19–23]. We focus on type-I WSMs due to their simplicity (i.e., only one pair of Weyl nodes in momentum space). In addition, the WSM-related experiments are generally performed at low temperatures and WSM sample sizes are typically on the nanometer scale [23,24]. These considerations can lead to difficulties in nonreciprocal experiments. So far, Weyl materials have been considered by the photonics community as candidates for nonreciprocal thermal emission in theoretical proposals involving geometries such as gratings [6,14], photonic crystals [25], and prisms [26]. In the majority of works, similar to previous studies with magneto-optical materials, patterned structures are used, where a resonant guided mode [6,10] or a polaritonic mode [14] is excited in the Voigt configuration [27]. Very recently, a broadband planar nonreciprocal structure was proposed [28].

Both material classes, magneto-optical materials and Weyl semimetals, are described via their dielectric permittivity tensor. In the Voigt configuration [14], this tensor takes the form

$$\epsilon_{\text{NR}} = \begin{pmatrix} \epsilon_d & 0 & \epsilon_{xz} \\ 0 & \epsilon_d & 0 \\ -\epsilon_{xz} & 0 & \epsilon_d \end{pmatrix}, \quad (1)$$

where $\epsilon_d \in \mathbb{C}$ and $\epsilon_{xz} = i\epsilon_a$ with $\epsilon_a \in \mathbb{R}$. For simplicity, we assume that the diagonal tensor elements are all equal. The nonzero imaginary ϵ_{xz} component results from an applied magnetic field (Weyl nodes separation) in magneto-optical materials (Weyl semimetals) along the y direction.

The number of nonzero tensor elements in the description of Eq. (1) makes the analytical description of nonreciprocal materials in the aforementioned inhomogeneous nano- and microstructures rather challenging. Here, in contrast to previous works relying heavily on numerical solvers, we derive simple analytical equations that describe how nonreciprocity

*georgia.papadakis@icfo.eu

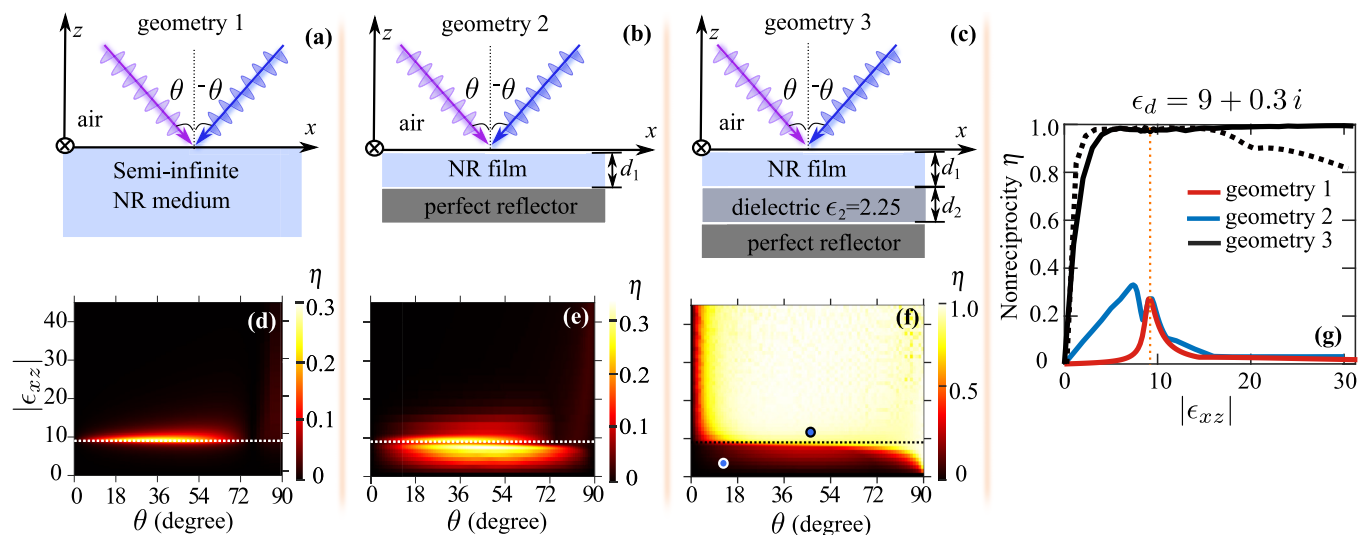


FIG. 1. Nonreciprocity in simple planar structures. We consider (a) a semi-infinite surface, (b) a NR film of thickness d_1 on a back reflector, and (c) a dielectric spacer separating a NR film from a back reflector. Color plots in (d)–(f) show the maximum nonreciprocity η within a wide range of thicknesses d_1 and d_2 for each geometry as a function of the off-diagonal tensor element of the nonreciprocal material (ϵ_{xz}) and the angle of incidence θ . Without loss of generality, we set $\epsilon_d = 9 + 0.3i$. The horizontal and vertical dashed lines indicate $|\epsilon_{xz}| = \text{Re}\{\epsilon_d\}$. For geometry 3 and panels (c) and (f), we set $\epsilon_2 = 2.25$. (g) Optimum η value in the maps of panels (d)–(f) as a function of $|\epsilon_{xz}|$. Solid curves represent results calculated with $\epsilon_d = 9 + 0.3i$, whereas the dashed curve corresponds to $\epsilon_d = -9 + 0.3i$ for geometry 3 (see more details in Sec. S4.A in SM [32]).

manifests itself in planar, pattern-free geometries. Previous works using gratings have achieved nonreciprocity values of $\eta \sim 0.4$ [10] and $\eta \sim 0.9$ [14] (see below for a detailed definition of η) with relatively large incidence angles. Our results suggest that planar structures can maximally violate Kirchhoff’s law, approaching the limit $\eta \sim 1$ for a wide range of incidence angles. We show that the considered configurations do not require the excitation of guided modes outside the light cone. In contrast, the near-complete violation of Kirchhoff’s law stems from wave interference as in conventional resonant absorption devices [29]. Finally, we numerically identify the minimum requirement for the off-diagonal permittivity tensor element ϵ_{xz} to produce a maximal violation of Kirchhoff’s law, and we classify currently available nonreciprocal materials in terms of this parameter.

We start by considering three standard planar geometries as shown in Fig. 1: A semi-infinite nonreciprocal medium [panel (a)], a nonreciprocal layer on a back reflector [panel (b)], and a dielectric spacer separating a nonreciprocal film from a back reflector [panel (c)]. A violation of Kirchhoff’s law suggests a difference between absorption and emission. For these nontransmissive geometries, $a_p(\theta) - e_p(\theta) = -[a_p(-\theta) - e_p(-\theta)] \in \{-1, 1\}$, where θ is the angle of incidence relative to the surface normal. In a practical thermal system, it should not matter whether $+\theta$ or $-\theta$ serves as the emission/absorption side. As a result, the nonreciprocity η can be simplified to $\eta = |a_p(\theta) - e_p(-\theta)| = |R(\theta) - R(-\theta)|$, which is equivalent to $|R(k_x) - R(-k_x)|$ [9,30,31], where the angle of incidence θ is shown in Figs. 1(a)–1(c), and k_x is the wave vector along x (for details see Sec. S2 in Supplemental Material, SM [32]). The reflectance is defined as $R = |r|^2$, where r is the reflection coefficient. In particular, in Fig. 1, the diagonal tensor element $\epsilon_d = 9 + 0.3i$ is chosen as an example.

The normal to the interfaces is aligned with the z axis. The layers of air, nonreciprocal material, and lossless dielectric, respectively, are labeled with subscripts 0–2. For example, $k_{z0} = \sqrt{k_0^2 - k_x^2}$ is the wave vector along z in the air. From momentum conservation, k_x remains the same in all the layers. In the bulk of the nonreciprocal material, one obtains four

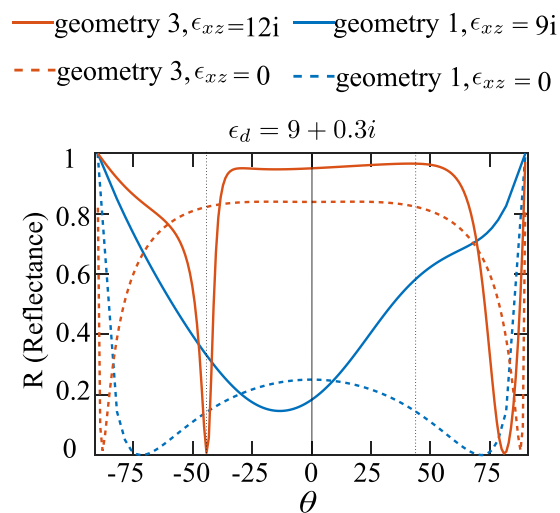


FIG. 2. Reflectance as a function of incidence angle θ for reciprocal ($\epsilon_{xz} = 0$, dashed curves) and nonreciprocal (solid curves, $\epsilon_{xz} \neq 0$) structures. Geometry 1 (blue curves) and geometry 3 (red curves) are chosen as examples. In particular, for geometry 3, the solid (dashed) curve corresponds to thicknesses $d_1/\lambda_0 = 0.10$, $d_2/\lambda_0 = 0.32$ ($d_1/\lambda_0 = 0.30$, $d_2/\lambda_0 = 0.11$). In the red solid curve, a maximum nonreciprocity $\eta = 0.96$ is obtained at $\theta = \pm 43^\circ$ (marked by vertical dashed lines; see Fig. 3 for details).

TABLE I. Parameter ranges for several available magneto-optical materials [see Eq. (1)] within the thermal emission wavelength range of 6–15 μm : InAs and GaAs under a magnetic field of 3 T, along with several Weyl semimetals in the absence of a magnetic field [marked with \times in the B(T) column]. Reported values correspond to room temperature unless otherwise stated.

Material		$\text{Re}\{\epsilon_d\}$	$\text{Im}\{\epsilon_d\}$	$ \epsilon_{xz} $	B (T)
Eu ₂ IrO ₇	[14,18]	–25–5	2	4–20	\times
Co ₃ Sn ₂ S ₂ (20 K)	[23,24]	20–40	20–40	25–45	\times
WSM standard (0 K)	[36]	–10–40	5–30	5–25	\times
InAs	[10]	3.6–10.9	2.1×10^{-2} – 3.4×10^{-1}	7.5×10^{-2} –1.2	3
GaAs	[37]	6.6–7.8	7.5×10^{-3} – 1.2×10^{-1}	1.0×10^{-2} – 1.7×10^{-1}	3

solutions for k_z , where two correspond to s -polarized fields and two to p -polarized fields (see Sec. S1 in SM [32]).

With the choice of the permittivity tensor of Eq. (1), s - and p -polarized electric fields are decoupled. In addition, the s -polarized fields do not experience any nonreciprocal response (see Sec. S1 in SM [32]). Thus, we focus here on p -polarized fields defined as $\mathbf{E}(\mathbf{r}, t) = 2\text{Re}\{(E_x, 0, E_z)\exp[i(\mathbf{k} \cdot \mathbf{r} - \omega t)]\}$ in the air, where $\mathbf{k} = (k_x, 0, k_z)$. It is then convenient to define $\epsilon_v = \epsilon_d - |\epsilon_{xz}|^2/\epsilon_d$, such that the z component of the wave vector in the nonreciprocal material is written as $k_{z1} = \sqrt{\epsilon_v k_0^2 - k_x^2}$.

First, we treat the problem fully analytically and derive the reflection coefficient for geometry 1 (see Secs. S1 and S3 in SM [32]),

$$r = \frac{k_{z0}\epsilon_v - k_{z1} + k_x\epsilon_{xz}/\epsilon_d}{k_{z0}\epsilon_v + k_{z1} - k_x\epsilon_{xz}/\epsilon_d}. \quad (2)$$

It is clear from Eq. (2) that $R(k_x) \equiv |r(k_x)|^2 \neq R(-k_x)$, even for the semi-infinite interface formed by the air and nonreciprocal material. Thus, this geometry in principle suffices to induce a nonreciprocal effect without spatial patterning or coupling to surface or guided modes. We note that by setting the denominator of Eq. (2) to zero, we obtain the surface plasmon dispersion relation $k_{z0}\epsilon_v + k_{z1} - k_x\epsilon_{xz}/\epsilon_d = 0$ [14,33,34], whereas by setting $\epsilon_{xz} = 0$, Eq. (2) reduces to the standard (reciprocal) Fresnel reflection coefficient for p

polarization. In Fig. 1(d), we show that there is an optimal value of ϵ_{xz} for maximal violation of Kirchhoff's law. Note that a larger ϵ_a does not necessarily lead to stronger nonreciprocity. In fact, for very large ϵ_{xz} , $R(k_x)$ and $R(-k_x)$ both approach unity, and thus, the nonreciprocity $\eta = |R(k_x) - R(-k_x)|$ vanishes. The same conclusion holds in geometries 2 and 3 (i.e., $\eta \rightarrow 0$ when $|\epsilon_{xz}| \rightarrow \infty$), although the values of $|\epsilon_{xz}|$ explored in Fig. 1(f) are not large enough to clearly observe this trend.

The reflection coefficient for geometry 2 is given by

$$r = \frac{\epsilon_{xz} k_x + i\epsilon_d k_{z1}/\tau_1 - (\epsilon_d k_0^2 - k_x^2)/k_{z0}}{\epsilon_{xz} k_x + i\epsilon_d k_{z1}/\tau_1 + (\epsilon_d k_0^2 - k_x^2)/k_{z0}} \quad (3)$$

with $\tau_1 = \tan(k_{z1}d_1)$ and d_1 is the thickness of the nonreciprocal material. Figure 1(e) indicates that the nonreciprocity η differs significantly from that of geometry 1. Furthermore, geometry 2 lacks tunability, because the absorption and phase of the reflected fields solely depend on the thickness of the nonreciprocal material slab.

To enhance the tunability in the design of the heterostructure, we insert a lossless dielectric layer with thickness d_2 below the nonreciprocal material, as shown by Fig. 1(c). This extra layer introduces an additional degree of freedom in optimizing the nonreciprocal thermal emitter, via imposing a tunable phase to the reflected fields. Thus, due to interference, the reflected fields, as well as the parameter η , are both strongly dependent on d_2 . We analyze geometry 3 through the expression

$$r = -\frac{(i\epsilon_{xz}\tau_2 k_{z2} - \epsilon_2 k_x)(k_x + \epsilon_{xz}k_{z0})/\epsilon_d + k_{z1}(\tau_2 k_{z2} - i\epsilon_2 k_{z0})/\tau_1 + (\epsilon_2 k_0^2 + i\epsilon_d \tau_2 k_{z2} k_{z0})}{(i\epsilon_{xz}\tau_2 k_{z2} - \epsilon_2 k_x)(k_x - \epsilon_{xz}k_{z0})/\epsilon_d + k_{z1}(\tau_2 k_{z2} + i\epsilon_2 k_{z0})/\tau_1 + (\epsilon_2 k_0^2 - i\epsilon_d \tau_2 k_{z2} k_{z0})} \quad (4)$$

with $\tau_2 = \tan(k_{z2}d_2)$. We note that Eq. (4) converges to Eq. (3) when setting $d_2 = 0$, and this in turn to Eq. (2) by taking the limit $d_1 \rightarrow \infty$. Further, we note that η vanishes if $\theta = 0$ or if $\epsilon_{xz} = 0$, as expected. Additionally, $\eta = 0$ when $\text{Im}\{\epsilon_d\}$ is zero (see Sec. S4 in SM [32]). This is also expected because a lack of optical loss prohibits thermal emission from the fluctuation-dissipation theorem [35]. As a rule of thumb, maximal violation of Kirchhoff's law ($\eta \sim 1$) can be obtained via the condition $|\text{Re}\{\epsilon_d\}| \leq |\epsilon_{xz}|$, provided that $|\epsilon_{xz}|$ is not too large as discussed above.

A nonreciprocity enhancement is observed over a broad range of incidence angles and off-diagonal permittivity values, as shown in Fig. 1(f). In Fig. 1(g), we demonstrate explicitly the dependence of η on $|\epsilon_{xz}|$ via selecting the maximum among all incidence angles in panels (d)–(f). We find that, for geometry 3, η approaches unity for considerably smaller values of $|\epsilon_{xz}|$ as compared to geometries 1 and 2. Thus, in practice, due to the typically small values of $|\epsilon_{xz}|$ that are available, for example in magneto-optical materials (see Table I), the three-layer geometry 3 is favorable. In Fig. 2,

we show the reflectance as a function of incidence angle for reciprocal and nonreciprocal instances of geometries 1 and 3, respectively. We conclude that the nonreciprocity is significantly enhanced through the addition of a dielectric spacer of optical thickness $d_2/\lambda_2 < 1$. Besides, a nonzero ϵ_{xz} leads to asymmetric reflection with respect to the incident angle θ for both geometries. In geometry 3, the nonreciprocity exhibits an asymmetric resonant response as a function of θ , which leads to stronger nonreciprocal effects in the optimal selection of $|\epsilon_{xz}|$ with respect to geometry 1, as shown in Fig. 1(g).

Based on the analytical expressions in Eqs. (2)–(4) for the reflection coefficient in the presence of nonreciprocity for the planar geometries 1–3, we can derive design rules for nonreciprocal thermal emitters. In particular, in Fig. 1(g), we demonstrate that geometry 3 requires a smaller value of $|\epsilon_{xz}|$ for achieving the same level of nonreciprocal response (η). Thus, henceforth, we focus on geometry 3 and evaluate in more detail Eq. (4).

We obtain results using the transfer-matrix method [38–41] (see Sec. S1 in SM [32]). Since the nonreciprocity η is a periodic function of d_1 and d_2 [Eq. (4)], we consider d_1/λ_1 and d_2/λ_2 in the range 0–3, as this range contains the sought-after maxima of η , where $\lambda_1 = \max(\text{Re}\{\lambda_0/\sqrt{\epsilon_v}\}, \text{Im}\{\lambda_0/\sqrt{\epsilon_v}\})$, $\lambda_2 = \lambda_0/\sqrt{\epsilon_2}$. Furthermore, we consider ranges of ϵ_d and $|\epsilon_{xz}|$ that correspond to known magneto-optical materials and Weyl semimetals within the thermal wavelength region of 6–15 μm at room temperature, as shown in Table I. The blackbody radiation at room temperature (300 K) is peaked around 10 μm . As a result, we choose to focus on the spectral range 6–15 μm , which contains the main part of the room temperature radiation (thermal radiation). The $\text{Co}_3\text{Sn}_2\text{S}_2$ (20 K) and WSM standard (0 K) are representative values for experimental and theoretical results, respectively [23,24,36].

In particular, we choose the calculation parameter ranges $\text{Im}\{\epsilon_d\} \in \{0.3, 3, 30\}$, $\text{Re}\{\epsilon_d\} \in [-35, 35]$, and $\text{Im}\{\epsilon_{xz}\} \in [0, 40]$. We note that, although only positive values of $\text{Im}\{\epsilon_{xz}\}$ are discussed here, negative $\text{Im}\{\epsilon_{xz}\}$ values are automatically accounted for because this is equivalent to rotating ϵ_{NR} in Eq. (1) by 180° around the z axis, which leads to invariant results by simultaneously flipping the signs of ϵ_{xz} and k_x . A value $\epsilon_2 = 2.25$ is chosen because it corresponds to a refractive index of 1.5, which represents well transparent dielectric materials such as quartz and glass. Other values of ϵ_2 can be chosen, which will not influence the conclusion of this paper. However, the corresponding optimal thicknesses will vary accordingly (see Figs. S7 and S8 in SM [32]). We note that the nonreciprocity is peaked at an intermediate value of ϵ_a , pointing towards the involvement of resonant modes assisting the nonreciprocal response at specific values of such parameter.

To understand the origin of the strong nonreciprocal response of geometry 3, in Fig. 3, we present the field profiles supported in this geometry for minimal and maximal violation of Kirchhoff's law, corresponding to $\eta = 0.05$ and $\eta = 0.96$, respectively. These values of nonreciprocity are represented in Fig. 1(f) by two blue dots. The parameter η is a periodic function of d_1/λ_0 and d_2/λ_0 . In Fig. 3 we consider values of d_1/λ_0 (vertical axes) varying from 0 to 0.4, including the first maximum of η . In particular, Figs. 3(a) and 3(b) show results for $\epsilon_{xz} = 12i$, $d_2/\lambda_0 = 0.32$, and $\theta = \pm 43^\circ$, where +

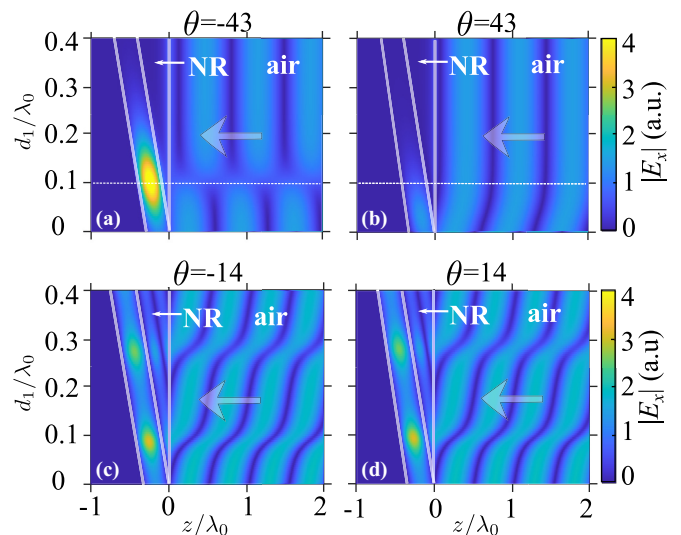


FIG. 3. Field profiles corresponding to the conditions marked by blue dots in Fig. 1(f) (geometry 3 with $\epsilon_d = 9 + 0.3i$). We plot the x -field amplitude as a function of the normalized distance z/λ_0 relative to the air/NR interface (horizontal axes) and normalized NR film thickness d_1/λ_0 (vertical axes). Thin white solid vertical lines indicate the interfaces in the planar structures. The white transparent arrow represents the field incidence direction. Panels (a) and (b) correspond to a nonreciprocity $\eta = 0.96$ with incidence angle $\theta = \pm 43^\circ$ and a dielectric spacer thickness $d_2/\lambda_0 = 0.32$. The vertical dashed line corresponds to the exact thickness selection in Fig. 2. Panels (c) and (d) correspond to $\eta = 0.05$ with $\theta = \pm 14^\circ$ and $d_2/\lambda_0 = 0.34$.

and $-$ correspond to $k_x > 0$ and $k_x < 0$, respectively. Figures 3(c) and 3(d) show field profiles calculated for $\epsilon_{xz} = 4i$, $d_2/\lambda_0 = 0.34$, and $\theta = \pm 14^\circ$. As clearly shown in Fig. 3, a maximal violation of Kirchhoff's law occurs when the field intensity is maximum inside the dielectric spacer. In other words, $\eta \sim 1$ is associated with a resonant mode inside the dielectric spacer, excited when light is incident from one side ($-k_x$), while it is suppressed when incident from the other side ($+k_x$). Since the transmission and reflection coefficients for $+k_x$ and $-k_x$ are not the same at WSM's interfaces, the maximum constructive/destructive interference condition for the entire heterostructure for $+k_x$ and $-k_x$ sides cannot be satisfied at the same time, leading to different overall reflection, (i.e., nonreciprocity).

Last, we analyze how material losses affect nonreciprocity by exploring three different values of $\text{Im}\{\epsilon_d\} \in \{0.3, 3, 30\}$, which span the entire parameter range in Table I, corresponding to realistic materials. In Fig. 4, we compute η when $\text{Re}\{\epsilon_d\}$ and ϵ_{xz} are varied. The parameter ranges of standard magneto-optical materials (GaAs and InAs) are shown in panel (a), whereas material properties representing Weyl semimetals Eu_2IrO_7 and $\text{Co}_3\text{Sn}_2\text{S}_2$ are shown in panels (b) and (c), respectively. For large $\text{Im}\{\epsilon_d\}$, the maximum of nonreciprocity tends to shift closer to $\theta \sim 90^\circ$ (i.e., grazing incidence, see Fig. S4 in SM [32]). The white contours in these figures represent the range of values of each labeled material as reported in recent literature [10,23,24,37]. From these figures, we have identified the degree of nonreciprocal response that each considered material can reach, upon optimizing d_1 and d_2 .

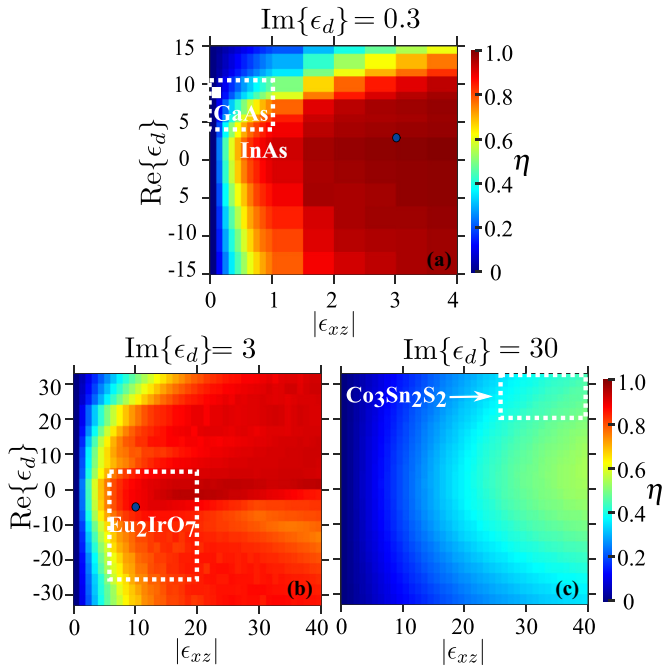


FIG. 4. Maximum nonreciprocity η for geometry 3 [Fig. 1(c)] as a function of the absolute value of the off-diagonal permittivity $|\epsilon_{xz}|$ and the real part of the diagonal permittivity $\text{Re}\{\epsilon_d\}$. Each data point is taken as the maximum value obtained when exploring the parameter space in d_1 , d_2 , and θ defined in the main text. In particular, we show two examples of materials within the explored range of parameters [marked by the blue dots in panels (a) and (b)], whose dependence on d_1 , d_2 , and θ in explored in Fig. S5 in SM [32].

In conclusion, we have shown that, even in a planar, pattern-free heterostructure, one can maximally violate Kirchhoff's law of thermal radiation. This can occur without the excitation of guided or polaritonic modes that lie outside the light cone. We described analytically how the off-diagonal tensor element in the permittivity of a nonreciprocal material (ϵ_{xz}) manifests itself in the reflection from a planar structure. Based on our theory, we show that the requirement for large values of ϵ_{xz} is relaxed in a three-layered geometry consisting of a nonreciprocal material on a dielectric spacer on a back reflector, whereas in a semi-infinite nonreciprocal material, a large value of ϵ_{xz} does not necessarily lead to stronger nonreciprocity. Our theory is general and applies to both magneto-optical materials and Weyl semimetals, which we have classified in our paper in terms of nonreciprocal thermal emission performance. Our analysis may serve to identify design rules for simpler nonreciprocal thermal emitters.

We thank Prof. Mehrdad Shokooh-Saremi, Prof. Bo Zhao, and Dr. Álvaro Rodríguez Echarri for stimulating discussions. L.W. thanks Mr. Juli Céspedes and Muhammad-Zeshan Sayab for IT-related discussions. This work has been supported in part by la Caixa Foundation (ID 100010434), the Spanish MICINN (PID2021-125441OA-I00, PID2020-112625GB-I00, and CEX2019-000910-S), the European Union (fellowship LCF/BQ/PI21/11830019 under the Marie Skłodowska-Curie Grant Agreement No. 847648), Generalitat de Catalunya (2021 SGR 01443), Fundació Cellex, and Fundació Mir-Puig.

- [1] Y. Xu, J. Li, Q. Tan, A. L. Peters, and C. Yang, Global status of recycling waste solar panels: A review, *Waste Manage.* **75**, 450 (2018).
- [2] M. A. Green, Time-Asymmetric Photovoltaics, *Nano Lett.* **12**, 5985 (2012).
- [3] Y. Park, Z. Omair, and S. Fan, Nonreciprocal thermophotovoltaic systems, *ACS Photonics* **9**, 3943 (2022).
- [4] P. T. Landsberg and G. Tonge, Thermodynamics and statistical mechanics, *J. Appl. Phys.* **51**, R1 (1980).
- [5] Y. Park, B. Zhao, and S. Fan, Reaching the ultimate efficiency of solar energy harvesting with a nonreciprocal multijunction solar cell, *Nano Lett.* **22**, 448 (2022).
- [6] Y. Park, V. S. Asadchy, B. Zhao, C. Guo, J. Wang, and S. Fan, Violating Kirchhoff's law of thermal radiation in semitransparent structures, *ACS Photonics* **8**, 2417 (2021).
- [7] C. Caloz, A. Alu, S. Tretyakov, D. Sounas, K. Achouri, and Z.-L. Deck-Léger, Electromagnetic Nonreciprocity, *Phys. Rev. Appl.* **10**, 047001 (2018).
- [8] S. Buddhiraju, A. Song, G. T. Papadakis, and S. Fan, Nonreciprocal Metamaterial Obeying Time-Reversal Symmetry, *Phys. Rev. Lett.* **124**, 257403 (2020).
- [9] L. Zhu and S. Fan, Near-complete violation of detailed balance in thermal radiation, *Phys. Rev. B* **90**, 220301(R) (2014).
- [10] K. J. Shayegan, B. Zhao, Y. Kim, S. Fan, and H. A. Atwater, Nonreciprocal infrared absorption via resonant magneto-optical coupling to InAs, *Sci. Adv.* **8**, eabm4308 (2022).
- [11] A. Figotin and I. Vitebsky, Nonreciprocal magnetic photonic crystals, *Phys. Rev. E* **63**, 066609 (2001).
- [12] B. Zhao, Y. Shi, J. Wang, Z. Zhao, N. Zhao, and S. Fan, Near-complete violation of Kirchhoff's law of thermal radiation with a 0.3 T magnetic field, *Opt. Lett.* **44**, 4203 (2019).
- [13] A. Kord, D. L. Sounas, and A. Alu, Microwave Nonreciprocity, *Proc. IEEE* **108**, 1728 (2020).
- [14] B. Zhao, C. Guo, C. A. Garcia, P. Narang, and S. Fan, Axion-field-enabled nonreciprocal thermal radiation in Weyl semimetals, *Nano Lett.* **20**, 1923 (2020).
- [15] Y. Wang, C. Khandekar, X. Gao, T. Li, D. Jiao, and Z. Jacob, Broadband circularly polarized thermal radiation from magnetic Weyl semimetals, *Opt. Mater. Express* **11**, 3880 (2021).
- [16] J. Wu, Z. Wang, H. Zhai, Z. Shi, X. Wu, and F. Wu, Near-complete violation of Kirchhoff's law of thermal radiation in ultrathin magnetic Weyl semimetal films, *Opt. Mater. Express* **11**, 4058 (2021).
- [17] S. Jia, S.-Y. Xu, and M. Z. Hasan, Weyl semimetals, Fermi arcs and chiral anomalies, *Nat. Mater.* **15**, 1140 (2016).
- [18] O. V. Kotov and Y. E. Lozovik, Giant tunable nonreciprocity of light in Weyl semimetals, *Phys. Rev. B* **98**, 195446 (2018).
- [19] N. Kumar, Y. Sun, N. Xu, K. Manna, M. Yao, V. Süss, I. Leermakers, O. Young, T. Förster, M. Schmidt *et al.*, Extremely high magnetoresistance and conductivity in the type-II Weyl semimetals WP_2 and MoP_2 , *Nat. Commun.* **8**, 1642 (2017).

- [20] X. Wan, A. M. Turner, A. Vishwanath, and S. Y. Savrasov, Topological semimetal and Fermi-arc surface states in the electronic structure of pyrochlore iridates, *Phys. Rev. B* **83**, 205101 (2011).
- [21] G. Xu, H. Weng, Z. Wang, X. Dai, and Z. Fang, Chern Semimetal and the Quantized Anomalous Hall Effect in HgCr_2Se_4 , *Phys. Rev. Lett.* **107**, 186806 (2011).
- [22] B. Yan and C. Felser, Topological materials: Weyl semimetals, *Annu. Rev. Condens. Matter Phys.* **8**, 337 (2017).
- [23] Y. Okamura, S. Minami, Y. Kato, Y. Fujishiro, Y. Kaneko, J. Ikeda, J. Muramoto, R. Kaneko, K. Ueda, V. Kocsis *et al.*, Giant magneto-optical responses in magnetic Weyl semimetal $\text{Co}_3\text{Sn}_2\text{S}_2$, *Nat. Commun.* **11**, 4619 (2020).
- [24] Y. Xu, J. Zhao, C. Yi, Q. Wang, Q. Yin, Y. Wang, X. Hu, L. Wang, E. Liu, G. Xu *et al.*, Electronic correlations and flattened band in magnetic Weyl semimetal candidate $\text{Co}_3\text{Sn}_2\text{S}_2$, *Nat. Commun.* **11**, 3985 (2020).
- [25] T. Li, C. Yin, and F. Wu, Strong optical non-reciprocity in one-dimensional photonic crystal containing a Weyl semimetal-based defect, *Opt. Mater.* **121**, 111583 (2021).
- [26] X. Wu, H. Yu, F. Wu, and B. Wu, Enhanced nonreciprocal radiation in Weyl semimetals by attenuated total reflection, *AIP Adv.* **11**, 075106 (2021).
- [27] D. Budker, W. Gawlik, D. Kimball, S. Rochester, V. Yashchuk, and A. Weis, Resonant nonlinear magneto-optical effects in atoms, *Rev. Mod. Phys.* **74**, 1153 (2002).
- [28] Z. Zhang and L. Zhu, Broadband Nonreciprocal Thermal Emission, *Phys. Rev. Appl.* **19**, 014013 (2023).
- [29] M. S. Ünlü and S. Strite, Resonant cavity enhanced photonic devices, *J. Appl. Phys.* **78**, 607 (1995).
- [30] Z. M. Zhang, X. Wu, and C. Fu, Validity of Kirchhoff's law for semitransparent films made of anisotropic materials, *J. Quant. Spectrosc. Radiat. Transfer* **245**, 106904 (2020).
- [31] J. Wu, F. Wu, T. Zhao, M. Antezza, and X. Wu, Dual-band non-reciprocal thermal radiation by coupling optical Tamm states in magnetophotonic multilayers, *Int. J. Therm. Sci.* **175**, 107457 (2022).
- [32] See Supplemental Material at <http://link.aps.org/supplemental/10.1103/PhysRevResearch.5.L022051> for details of the transfer-matrix method; the connection between reflection, emissivity, and absorptivity; a derivation of Eq. (2); and the influence of the diagonal permittivity tensor element on nonreciprocity.
- [33] B. Hu, Y. Zhang, and Q. J. Wang, Surface magneto plasmons and their applications in the infrared frequencies, *Nanophotonics* **4**, 383 (2015).
- [34] K. Chiu and J. Quinn, Magnetoplasma surface waves in metals, *Phys. Rev. B* **5**, 4707 (1972).
- [35] L. Mandel and E. Wolf, *Optical Coherence and Quantum Optics* (Cambridge University Press, Cambridge, 1995), Chap. 17.2.
- [36] Q. Chen, A. R. Kutayiah, I. Oladyshkin, M. Tokman, and A. Belyanin, Optical properties and electromagnetic modes of Weyl semimetals, *Phys. Rev. B* **99**, 075137 (2019).
- [37] H. Wang, H. Wu, and J.-Q. Zhou, Nonreciprocal optical properties based on magneto-optical materials: n-InAs, GaAs and HgCdTe, *J. Quant. Spectrosc. Radiat. Transfer* **206**, 254 (2018).
- [38] T. G. Mackay and A. Lakhtakia, The transfer-matrix method in electromagnetics and optics, *Synthesis Lectures on Electromagnetics* **1**, 1126 (2020).
- [39] D. W. Berreman, Optics in Stratified and Anisotropic Media: 4×4-Matrix Formulation, *J. Opt. Soc. Am.* **62**, 502 (1972).
- [40] N. C. Passler and A. Paarmann, Generalized 4×4 matrix formalism for light propagation in anisotropic stratified media: study of surface phonon polaritons in polar dielectric heterostructures: Erratum, *J. Opt. Soc. Am. B* **34**, 2128 (2017).
- [41] P. Yeh, Electromagnetic propagation in birefringent layered media, *J. Opt. Soc. Am.* **69**, 742 (1979).